journal of
nuclear
materials

Effects of proton irradiation on the microstructure and microchemistry of type 304L stainless steel

R.D. Carter [a], D.L. Damcott [a], M. Atzmon [a], G.S. Was [a] and E.A. Kenik [b]

[a] Department of Nuclear Engineering, University of Michigan, Ann Arbor, MI 48109, USA
[b] Metals and Ceramics Division, Oak Ridge National Laboratory, Oak Ridge, TN 37831-6376, USA

A research program has been undertaken to determine the origins of irradiation-assisted stress corrosion cracking (IASCC) in austenitic alloys in light water reactors, and the effect of impurities on IASCC susceptibility. Controlled purity alloys of 304L stainless steel were irradiated with protons at 400°C to a dose of 1 dpa and analyzed via Auger electron spectroscopy (AES) and scanning transmission electron microscopy (STEM). The alloys investigated were an ultra-high purity (UHP) alloy and UHP alloys containing phosphorus (UHP + P), sulfur (UHP + S), or silicon (UHP + Si). Microstructural and microchemical changes were quantified and compared with literature results for other irradiating species. Following irradiation, the alloys showed dislocation loop formation and growth, "black dot" loops, and a change in the nature of the dislocation network. AES and STEM microchemical analysis of the alloys revealed Cr depletion of up to 6 at% and Ni enrichment of up to 6.6 at% at the grain boundaries of the alloys, with more segregation observed in the alloys containing impurities than in the UHP alloy. Significant grain boundary enrichment of P and Si in the UHP + P and UHP + Si alloys, respectively, was also observed. The results of the analyses of proton-irradiated samples are shown to compare favorably with previous studies on samples irradiated with neutrons at or near LWR conditions.

1. Introduction

Irradiation-assisted stress corrosion cracking (IASCC) is a phenomenon which has come under significant scrutiny in the last decade [1–4] because it continues to be a problem in light water reactor (LWR) core components. Exposure to neutron radiation in the reactor core leads to changes in the microstructure and microchemistry of austenitic alloys [2–6], which are suspect in the enhancement of the intergranular stress corrosion cracking (IGSCC) process. The specific mechanisms controlling IASCC susceptibility have yet to be identified due to the difficulties and expense involved in studying neutron-irradiated alloys. The high residual activity resulting from neutron irradiation requires that samples either be allowed to decay for extended periods of time or that experiments be conducted entirely within hot cells [7–10], procedures which add significantly to the cost and time scale involved in the analyses. Irradiation with heavy ions has an advantage over neutrons in that the resulting activation is relatively low and that a much shorter time is necessary to reach desired levels of damage; however, the shallow depth of penetration of these

ions makes the study of grain boundary segregation and microstructural changes in the bulk exceedingly difficult.

These problems can be overcome by irradiating alloys with light ions to induce microstructural and microchemical changes similar to those created by in-core irradiations. Protons with energies of a few MeV appear ideal for this purpose for a variety of reasons. Irradiation to damage levels of interest can be achieved in a few days, as opposed to the years necessary for similar levels of neutron damage; 3.4 MeV protons have ranges on the order of 40 μm, which, combined with a small grain size, allows study of grain-boundary related effects; the damage profile is nearly flat over most of the proton range; and there is relatively little residual activity after irradiation. The irradiation damage is dependent upon the displacement rate during irradiation. Because protons have a higher displacement rate than neutrons, higher temperatures are necessary to retain the same residual concentrations of defects in proton irradiated stainless steels [11].

It has been suggested that IASCC susceptibility is strongly dependent upon grain boundary composition and is therefore affected by impurity and major ele-

ment segregation. Radiation-induced segregation (RIS) of silicon or phosphorus to the grain boundaries has been suggested as the origin of IASCC [9,12]. Andresen [11] suggests that the depletion of chromium at the boundaries is necessary for IASCC to occur. In addition, changes in the microstructure due to irradiation may have significant effects on the deformation behavior of the material.

This paper presents the experimental techniques and results of the microstructural and microchemical development following proton irradiation of austenitic alloys with controlled impurity concentrations. To compare with grain boundary compositions created at LWR irradiation conditions at 288°C, proton irradiation temperatures of 400°C were used in this study to induce the same amount of grain boundary segregation [3]. A comparison is made between microstructures and chemical redistribution formed during 3.4 MeV proton irradiation and those formed in-core in nuclear reactors. The results serve as a basis upon which results from stress corrosion cracking experiments on the same alloys can be analyzed and interpreted with regard to cracking and deformation behavior, susceptibility to IASCC, and intergranular crack propagation, in hopes of further understanding IASCC in nuclear reactors.

2. Experimental procedure

Four controlled-purity alloys of type 304L stainless steel were examined: an ultra-high purity alloy (UHP) and ultra-high purity alloys containing additions of 0.03 at% sulfur (UHP + S), 0.08 at% phosphorus (UHP + P), or 0.87 at% silicon (UHP + Si). The base compositions of these alloys, as determined by electron microprobe analysis, are given in table 1.

The as-received alloys were solution annealed at 1100°C to produce a homogeneous microstructure and microchemistry. This resulted in a grain size of 100–200

μm. The alloys were cold-rolled from a thickness of 20 mm to 2 mm to provide a reduced grain size upon recrystallization. The material was then cut into samples having a 4 × 2 mm cross section for examination by electron microscopy, or a 2 × 2 mm cross section for Auger electron spectroscopy (AES) analysis. AES samples were notched on one side to aid in stress concentration during fracturing. These samples were wet polished using 320 to 600 grit silicon carbide paper and then recrystallized by annealing in flowing argon at 850°C for 1 h for the UHP alloy or 0.5 h for all other alloys to achieve a final grain size of 5–15 μm. After annealing, the samples were wet polished using 1200 and 2400 grit SiC paper and were electropolished in a solution of 60% phosphoric acid and 40% sulfuric acid at 7 V for 5 min to provide a smooth surface prior to irradiation.

All samples were irradiated using 3.4 MeV protons in a specially designed isolated sample irradiation stage. As protons of this energy produce a region of nearly-uniform damage over the first 30 μm of the proton range, all irradiations were carried out to a total dose of 1 dpa in this region at a dose rate of approximately 7.0×10^{-6} dpa/s. The sample temperature during irradiation was controlled at 400° ± 10°C by simultaneous resistive heating and air-cooling of the stage, and was monitored by a calibrated infrared pyrometer. A thin foil of pure tin was sandwiched between the samples and the stage, because tin is liquid at the irradiation temperature, providing good thermal contact between the samples and the stage for efficient temperature control. Following irradiation, the proton-induced residual activity decayed to near-background levels within 72 h, allowing for safe sample analysis. Measurements of unirradiated compositions in AES were conducted on the unirradiated back side of the irradiated samples, and in STEM were conducted on TEM disks taken from the back half of the irradiated samples. This was to ensure comparable thermal and

Table 1
Bulk alloy compositions in atomic percent as determined by electron microprobe analysis

Alloy	Cr	Ni	Mn	Al	S	P	Si	Fe [b]
UHP	20.72	8.88	1.11	0.02	ND [a]	0.01	0.09	69.17
UHP + S	20.91	8.94	1.04	ND	ND [c]	ND	0.03	69.08
UHP + P	21.02	8.68	1.15	ND	ND	0.08	0.03	69.04
UHP + Si	20.41	8.55	1.34	ND	ND	ND	0.87	68.83

[a] ND: Element was not detected in electron microprobe analysis.

[b] Fe concentration determined such that the sum of all elements = 100%.

[c] Element was not detected in electron microprobe analysis, nominal composition 0.03 at%.

mechanical histories were maintained in both sample conditions.

Three millimeter disk samples for STEM analysis were cut using a slurry drill core cutter to minimize introduction of external deformation. These samples were mechanically back-thinned to approximately 100 μm thickness, followed by electrochemical jet thinning to achieve foil regions which were electron-transparent. The thinning solution used was 20 vol% perchloric acid in ethanol at a constant voltage of 120 V and temperature of −50°C. Microstructural analysis was performed using a JEOL 2000FX STEM/TEM, a Philips EM420 TEM, and a Philips CM12 STEM/TEM, all of which are part of the University of Michigan Electron Microbeam Analysis Laboratory (EMAL). Microchemical analysis on the STEM was performed on a Philips EM400T/FEG at Oak Ridge National Laboratory. EDS analysis in the EM400T/FEG was done using a 2 nm incident probe in STEM mode in regions of sample thickness less than 100 nm.

Microstructural analysis was performed using standard techniques. Dislocation line density was measured using the line-intercept and surface-intersection methods [13]. For this purpose, foil thicknesses were determined using CBED and the modified IMAGE computer program [14]. Densities of dislocation loops, black dots, and precipitates, as well as sizes of dislocation loops, were obtained directly from bright- and weak-beam dark-field micrographs of known area and sample thickness [15]. Determination of Burgers vectors, loop types, and stacking fault types were made using techniques as detailed by Loretto and Smallman [16]. For good statistical accuracy, 50 loops in the UHP alloy and 20 loops in each of the other alloys, were analyzed to determine dislocation loop type. Over 1000 loops and "black dot" loops were included in the density calculations for each alloy, and more than 300 loops were used in the loop size determination per alloy.

STEM/EDS measurements were made at numerous grain boundaries, and also in 1.67 to 2.5 nm increments away from the boundaries to provide composition profiles as a function of distance from the boundary. Scatter in these measurements was expected to result primarily from three sources: differences in the structure of grain boundaries from one boundary to the next resulting in differences in segregation, sample drift leading to broader and shallower boundary profiles, and error due to difficulties in achieving precise alignment of the grain boundary with the incident beam. No account for the broadening of the profile due to the size of the beam-interaction volume within the foil is presented in this work, but is included in a future publication [17].

To promote intergranular fracture upon loading, samples for Auger spectroscopic analysis were cathodically charged with hydrogen after irradiation according to the procedure described by Briant [18]. Charged samples were fractured in situ in the Perkin Elmer (PHI) 660 scanning Auger microprobe (SAM) chamber at approximately 0°C. Notched samples were loaded in the fracture stage and held firmly just below the notch. Fracture was achieved by inserting the fracture arm slowly to bend the sample over by 45° within 7 min, exposing grain facets on the irradiated and unirradiated faces of the sample. Spectra of intensity as a function of Auger electron energy were collected from exposed grain boundaries by surveying all the Auger electron energies from 0 to approximately 2100 eV to identify the species present, and then using the multiplex option on the SAM to scan only the energy intervals of the elemental peaks. The elements used for multiplex analysis were iron, chromium, and nickel in all samples, and sulfur or phosphorus in the doped material. Additionally, contamination by carbon and oxygen was monitored continuously during data acquisition by including the elemental peaks during multiplexed acquisitions. Data collection was terminated when carbon and oxygen peaks became distinguishable from background noise, having concentrations estimated to be less than 5 at%. All spectra were collected using a beam voltage of 10 kV with a beam current of 5 nA at pressures better than 7.0×10^{-9} Torr. The spectra were differentiated with respect to energy. The atomic concentration routine in the spectrometer operating software was used to convert intensity to atomic concentration following the procedure as outlined in the Handbook of Auger Electron Spectroscopy [19]. Further details of the AES sample preparation and measurement procedures have been reported previously [20].

3. Results and discussion

3.1. Microstructure

The microstructures of all of the unirradiated alloys were nearly identical. Average grain diameters were 10–12 μm for the UHP and 7–9 μm for the UHP + P, UHP + S, and UHP + Si samples, with no observable change following irradiation. These diameters were chosen because they provide 3–5 grains in a cross

section of the uniform damage region, allowing for nearly polycrystalline behavior and "bulk" characterization with little influence of surface effects. Approximately 10–20% of the observed grains were unrecrystallized, and contained dense tangles of dislocations. In addition, some of these regions were observed to contain martensite. Presumably the martensite formed via transformation of the austenite during the jet electropolishing of the TEM disks at low temperature. Indeed, this transformation was observed in situ at low temperatures in STEM during microchemical analysis using a cold stage at temperatures below −40°C. These regions were not included in the dislocation analysis. As expected, no dislocation loops were present in the unirradiated state. Annealing twins and intrinsic and extrinsic stacking faults (with displacement vectors of $\pm \frac{1}{3}\langle 111 \rangle$) were observed as are commonly found in a face-centered cubic structure.

The microstructural changes upon irradiation are summarized in table 2, and described in the following paragraphs. The most dramatic effect of irradiation was seen in the dislocation structure. Before irradiation (fig. 1) a loose dislocation network is observed with a density of approximately 10^{13} m^{-2} in the alloys. The lack of preferred orientation for the dislocations indicated that the recrystallization anneal was effective at eliminating the majority of the cold-work introduced by the cold-rolling process. In addition, dislocations on grain boundaries and extended dislocations (with stacking faults in between) were present. After proton irradiation, the dislocation microstructure changed dramatically, as can be seen in the UHP + P alloy in fig. 2 which is at nearly the same magnification as fig. 1. Fig. 3 shows the microstructure of the irradiated UHP + P alloy in detail. The fine scale damage was observed as resolvable dislocation loops, "black dot" loops, and short dislocation line segments, the three features which dominate the irradiated microstructure in each
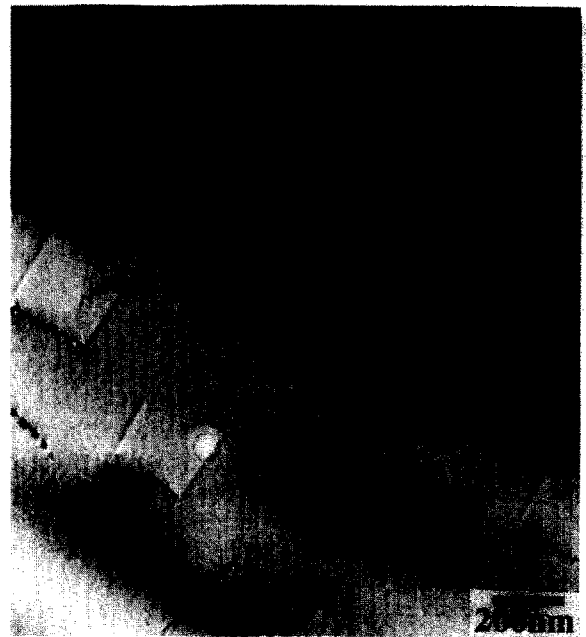

Fig. 1. Bright-field TEM micrograph of dislocations in the unirradiated UHP + P alloy.

alloy. There was no defect-free or denuded region around the grain boundaries or twin boundaries in any of the alloys, nor was any radiation-induced precipitation found in any of the alloys.

Dislocation loops were the first microstructural feature observed after irradiation. As seen in fig. 4a, a weak-beam dark field TEM micrograph showing the dislocation loops and other defects in the irradiated UHP + P material, the loops in the UHP + P alloy vary in size, consistent with the other alloys as well. The density of dislocation loops was 5.7×10^{21} m^{-3} in the UHP and UHP + P alloys, 9.5×10^{21} m^{-3} in the UHP

Table 2
Pre- and post-irradiation microstructures of UHP, UHP + P, UHP + S, and UHP + Si alloys

	Alloy/condition				
	UHP/SA [a]	UHP/IRR [b]	UHP + P/IRR	UHP + S/IRR	UHP + Si/IRR
Grain size	10–12 μm	10–12 μm	7–9 μm	7–9 μm	7–9 μm
Faulted loop size	None	16 ± 9 nm	27 ± 13 nm	14 ± 8 nm	10 ± 7 nm
Dislocation Density					
Network	1.6×10^{13} m^{-2}	2.2×10^{14} m^{-2}	2.0×10^{14} m^{-2}	2.0×10^{13} m^{-2}	9.8×10^{13} m^{-2}
Loops	None	5.6×10^{21} m^{-3}	5.7×10^{21} m^{-3}	9.4×10^{21} m^{-3}	1.0×10^{22} m^{-3}
Black dot loops	None	6.7×10^{21} m^{-3}	8.0×10^{21} m^{-3}	9.6×10^{21} m^{-3}	1.3×10^{22} m^{-3}

[a] SA = Unirradiated alloy, microstructure is the same for all unirradiated alloys.
[b] IRR = Irradiated alloy.

+ S alloy, and 1.0×10^{22} m^{-3} in the UHP + Si alloy. The main difference between the alloys was faulted loop size. These loops had average diameters of 16 ± 9 nm (UHP), 27 ± 13 nm (UHP + P), 14 ± 8 nm (UHP + S), and 10 ± 7 nm (UHP + Si). The resolvable loop diameters ranged from about 5 nm to as large as 50 nm, irrespective of alloy. For all of these alloys more than 85% of the loops were Frank (faulted) in nature ($b = \frac{1}{3}\langle 111 \rangle$), the remainder, which generally tended to be larger, were perfect loops ($b = \frac{1}{2}\langle 110 \rangle$). All of the dislocation loops analyzed were interstitial in nature.

"Black dot" loops were the second feature found in the irradiated samples. These small regions of contrast, as seen in fig. 4b, are small dislocation loops, the nature of which is unresolvable by ordinary means. The "black dot" loops were observed at densities of 6.7×10^{21} m^{-3} (UHP), 8.0×10^{21} m^{-3} (UHP + P), 9.5×10^{21} m^{-3} (UHP + S), and 1.3×10^{22} m^{-3} (UHP + Si). These densities are slightly higher than the resolvable dislocation loop densities for each alloy. These may be very small interstitial loops that have recently been nucleated, and also small vacancy loops which have formed from the collapse of collision cascades and which have
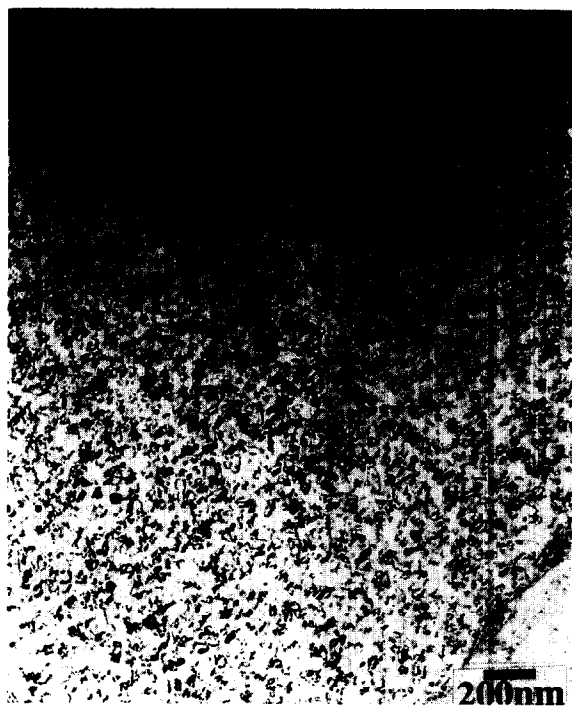

Fig. 3. Higher magnification weak-beam dark-field TEM micrograph displaying faulted dislocation loops and "black dot" loops in a UHP + P sample irradiated with 3.4 MeV protons to 1 dpa at 400°C.

Fig. 2. Low magnification bright-field TEM micrograph of the microstructure in the UHP + P alloy irradiated with 3.4 MeV H$^+$ at 400°C to 1 dpa.

not yet absorbed enough interstitials to be annihilated. This is consistent with the observations of Fukushima [21] who found that during irradiation the stronger loop bias for interstitials compared with vacancies will result in vacancy loop shrinkage due to the net influx of interstitials, while the interstitial loops will grow.

The long, loose dislocations present before irradiation were not observable afterward, instead, the visible line dislocations were short segments. These segments may be the result of the unfaulting of dislocation loops or may be the remnants of the longer dislocations present before irradiation. The network dislocation density increased by nearly an order of magnitude in the UHP, UHP + P, and UHP + Si alloys, but only increased slightly in the UHP + S alloy. A typical dislocation segment is shown in fig. 4c, in this case found in the UHP + P alloy.

IASCC of reactor core components has not been observed in the field below fluences of around 0.6 dpa [12]. Because the goal of the present study is to reproduce the radiation damage observed in LWR core components, a comparison with neutron irradiation

studies of (preferably 304) austenitic stainless steel, at 250–300°C and 0.6–5 dpa is sought. Because of the scarcity of microstructural data, reports on studies at higher temperatures and doses, as well as for 316SS or PCAs (fusion primary candidate alloys), will also be used for comparison. For experiments conducted at the same temperature, the dose is expected to have only a weak effect on loop size and density above 0.1 dpa [22].

The work of Bloom et al. [23] (~ 1 dpa) on 304SS, Maziasz [24] and Hamada et al. [25] on 316SS at higher doses, and Tanaka et al. [26], Hamada et al. [25], and Suzuki et al. [27] on PCAs at higher doses all confirm
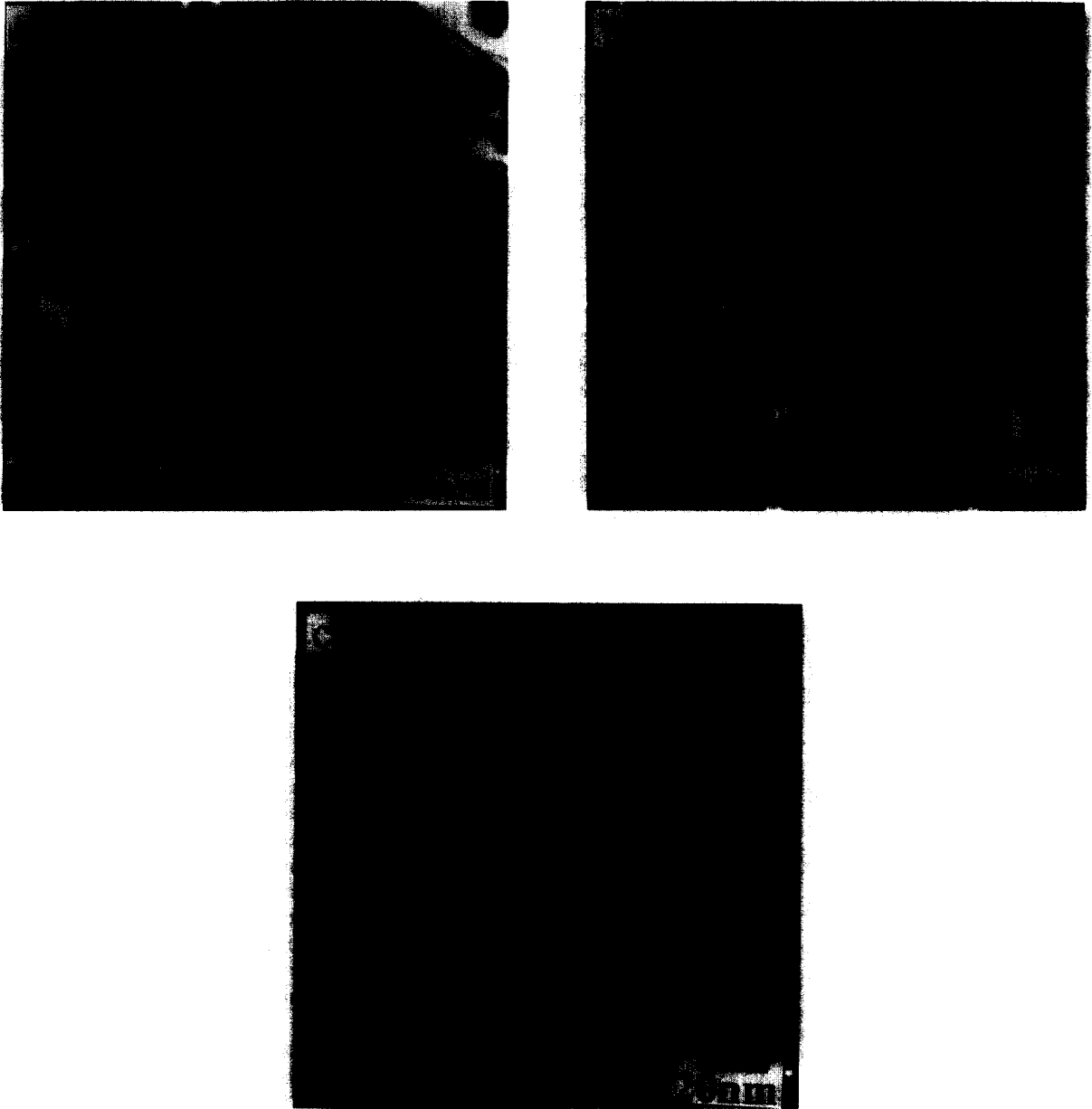
Fig. 4. Weak-beam dark-field TEM micrographs showing the microstructural features in the UHP + P alloy irradiated with 3.4 MeV H$^+$ at 400°C to 1 dpa, as indicated by arrows: (a) dislocation loops, (b) "black dot" loops, and (c) dislocation line segments.

that irradiation with neutrons at 300°C results in loop sizes of 9–20 μm independent of dose or alloy. This compares favorably with the 10–16 μm loop diameters found in the proton-irradiated UHP, UHP + S, and UHP + Si alloys. However, the UHP + P loop diameter of 27 μm is considerably larger than that found in neutron irradiations. Unfortunately, Bloom et al. only report the loop density as "high," providing no quantitative information. Loop densities reported by the other authors above are all in the 10^{22} m^{-3} range with concentration decreasing with increasing dose. The loop densities in the present study [$(0.5–1) \times 10^{22}$ m^{-3}] are slightly smaller than those found in neutron-irradiated alloys. This is likely due to the higher irradiation temperature necessary to produce similar segregation levels in the present study, as it has been found in neutron irradiations [22] that the loop density decreases with increasing temperature. Maziasz [24] reported black dot densities of 3.7×10^{22} m^{-3} in 316SS irradiated to 7.8 dpa with neutrons at 55°C. Bloom et al. [23] observed no precipitation due to irradiation at 1 dpa and 300°C, nor did Maziasz and McHargue [22] observe precipitation in this dose and temperature range (less than 400°C and 5 dpa) in their review of neutron irradiation of austenitic alloys.

3.2. Microchemistry

Table 3 summarizes the grain boundary compositions of each alloy as measured by AES and/or STEM/EDS. Fig. 5 displays the differences in the
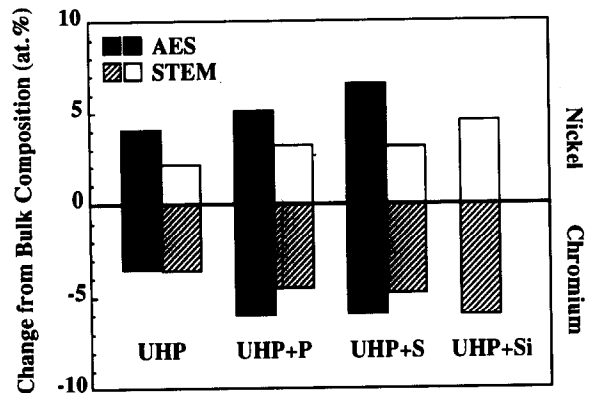

Fig. 5. Changes in the grain boundary concentration from the bulk levels for Cr and Ni for the UHP, UHP + S, UHP + P, and UHP + Si alloys irradiated with 3.4 MeV H$^+$ at 400°C to 1 dpa, as measured by AES and/or STEM/EDS. STEM/EDS values are the average of all grain boundary measurements, not just from the profiled grain boundaries.

major element compositions at the boundary as a change from the bulk alloy composition after irradiation. Because intergranular fracture was not achieved in the unirradiated UHP and UHP + S alloys, grain boundary measurements in unirradiated samples were not possible. It has been assumed that these grain boundary compositions were the same as the bulk compositions. Comparison of grain boundary compositions to the bulk composition was made in the UHP + P alloy for consistency with the other alloys. As significant thermal segregation would not be expected at

Table 3
Summary of AES and STEM measurements of grain boundary composition of alloys UHP, UHP + S, UHP + P, and UHP + Si (in at%). Errors are given as the standard deviation of the mean, $\sigma / \sqrt{N}$

Alloy	Number of measurements	Number of samples	Number of batches	Fe	Cr	Ni	P	S	Si
UHP									
Irradiated (AES)	31	5	3	69.9±0.7	17.2±0.7	12.9±0.3	ND [a]	ND	ND
Irradiated (STEM)	26	2	2	71.5±0.1	17.1±0.2	11.0±0.2	ND	ND	ND
UHP + S									
Irradiated (AES)	42	5	2	69.3±0.5	15.0±0.5	15.5±0.5	ND	ND	ND
Irradiated (STEM)	18	1	1	71.4±0.1	16.1±0.2	12.0±0.2	ND	ND	ND
UHP + P									
Irradiated (AES)	34	7	3	62.5±0.7	15.0±0.4	13.8±0.5	8.7±0.4	ND	ND
Irradiated (STEM)	14	1	1	70.2±0.3	16.5±0.4	11.9±0.3	1.4±0.1	ND	ND
Unirradiated (AES)	8	4	2	64.3±1.0	21.7±0.7	8.8±0.5	5.3±0.4	ND	ND
UHP + Si									
Irradiated (STEM)	21	1	1	69.3±0.2	14.4±0.2	13.1±0.2	ND	ND	3.2±0.1

[a] ND: not detected.

400°C [28,29], any changes in the grain boundary composition in the irradiated alloys were assumed to be due to irradiation. AES analysis of the UHP + Si alloy was impossible due to inability to achieve intergranular fracture in this alloy.

Significant differences in grain boundary composition as compared to the bulk composition were observed via AES in the irradiated UHP, UHP + S, and UHP + P alloys, as well as the unirradiated UHP + P alloy. The UHP alloy showed chromium depletion to 17.2 at% at the boundary from 20.7 at% in the bulk. Nickel was enriched to 12.9 at% from 8.9 at% in the bulk material. There was a very slight increase in the iron concentration (+0.7 at%) at the boundary as compared to the bulk alloy.

Both the UHP + S and UHP + P alloys showed more dramatic redistribution of Cr and Ni at the grain boundaries under irradiation, possibly indicating a synergistic relationship between these elements and the impurities. The Cr concentration in the UHP + S alloy dropped from 20.9 to 15.0 at% at the boundary, and from 21.0 to 15.0 at% at the boundary in the UHP + P alloy. Nickel was enriched from 8.9 to 15.5 at% and from 8.7 to 13.8 at% in the UHP + S and UHP + P alloys, respectively. There was very little change in the grain boundary Fe concentration in the UHP + S alloy. However, in the UHP + P alloy, the Fe concentration at the boundary decreased by 6.6 at% from the bulk concentration of 69.0 at%. Because the alloys showing no impurity segregation have little change in the grain boundary Fe concentration, and the Cr and Ni changes are approximately equal and opposite, this decrease in the grain boundary Fe concentration is likely to be due to displacement by phosphorus.

Phosphorus enrichment at the grain boundary to an average level of 8.7 at% was observed in the irradiated UHP + P alloy. This is an increase to greater than 1.6 times the grain boundary concentration in the unirradiated material and 100 times the bulk value of 0.08 at%. No enrichment of sulfur was measured at the boundaries of the UHP + S alloy. This is consistent with previous observations that radiation-induced S segregation can be difficult to detect in commercial stainless steel alloys [3]. Additionally, the very low overall S concentration in the alloy used in this study increases this difficulty. The fact that S was not observed to segregate at the boundary (less than the detection limit of 1–1.5 at%) indicates that large quantities of impurities need not segregate to the boundary for increased Cr and Ni redistribution to occur. Much more information regarding the segregation behavior of complex alloys must be known before the dependence of Cr and

Ni redistribution on impurity additions to the alloy can be explained.

Phosphorus segregation was also measured in the unirradiated UHP + P alloy. The increase in the P to a level of 5.3 at% at the boundary was due to thermal segregation during the recrystallization heat treatment at 850°C. This amount of P segregation is consistent with previous observations in stainless steel [29] and nickel-based alloys [30,31]. The thermal segregation of phosphorus was accompanied by a similar decrease in the Fe concentration at the grain boundary (4.7 at% decrease). Chromium was enriched slightly (0.6 at% increase) at the boundary, consistent with the observations of James and Shepherd [32] in thermally treated type 316 stainless steel. There was virtually no change in the grain boundary Ni concentration. Auger analysis of the UHP and UHP + S alloys in the unirradiated condition and the UHP + Si alloy in either the irradiated or unirradiated conditions was not possible because no intergranular facets were exposed.

The grain boundary compositions in the alloys were also measured by scanning transmission electron microscopy (STEM). In figs. 6–9, the measured segregation profiles for Fe, Ni, Cr, and any minor elemental additions detected are shown for the four alloys. Measurements of grain boundary composition were made in each alloy on many different grain boundaries, and two or three grain boundaries were chosen for full profiles in each case.

The measured profiles for two grain boundaries from the UHP alloy are shown in fig. 6. The average concentrations of Fe, Cr, and Ni for the two boundaries are 71.5, 17.1, and 11.0 at% respectively, and, as with all of the alloys, the average full widths at half maximum (FWHM) are 3 to 6 nm. The values for the grain boundary compositions compare well with the AES measured values of 17.2 at% in Cr, but for Ni AES measures 12.9 at% at the boundary. The Fe enrichment of 2.3 at% is greater than the enrichment of 0.7 at% detected by AES.

Fig. 7 shows the measured profiles for Fe, Cr, Ni, and P in the UHP + P alloy. At the boundary, an average Cr level of 16.5 at% was observed, versus 15.0 at% by AES, and an average Ni level of 11.9 at%, versus 13.8 at% by AES. The P profile had a peak grain boundary concentration of 1.4 at% as compared to 8.7 at% by AES. Significant Fe enrichment was not detected at the grain boundary by AES, but enrichment was observed by STEM, with a 0.8 at% increase over bulk levels at the grain boundary. This is significantly less than the regions surrounding the boundary, and is a result of the displacement by P at the bound-
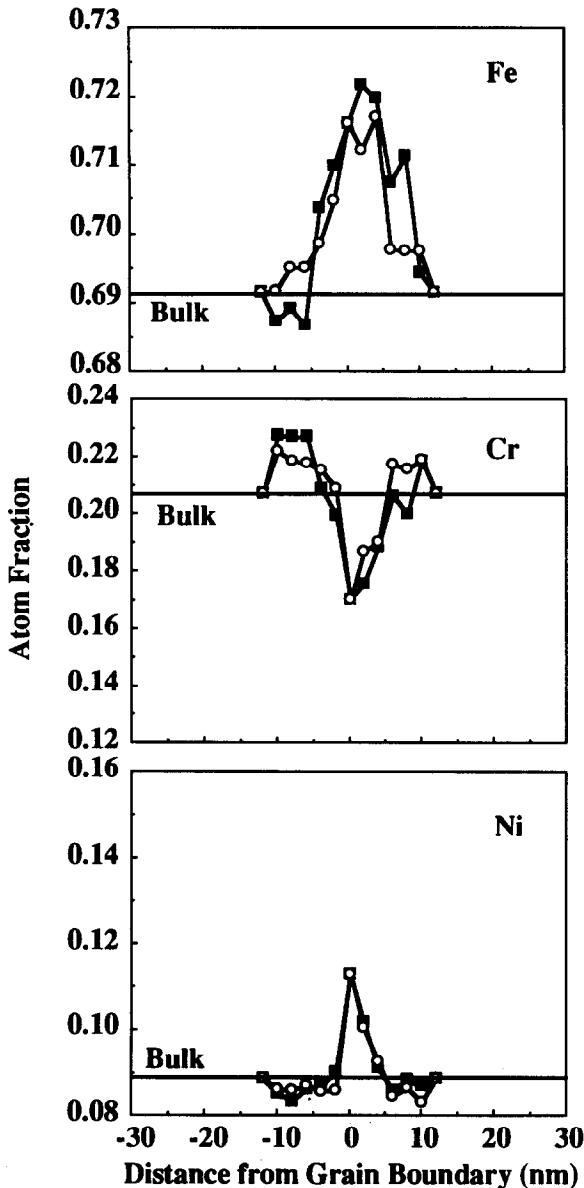
The profiles of Fe, Cr, and Ni for 3 grain boundaries of the UHP + S alloy are shown in fig. 8. No sulfur segregation to the grain boundary was detectable by STEM/EDS in this alloy. Cr levels of 16.1 at% are again slightly higher than the AES measured value of 15 at%, and the STEM Ni level of 12.0 at% is significantly less than the 15.5 at% detected in AES. Iron enrichment of 2.3 at% was found at the boundary, compared with little Fe redistribution found by AES.

In fig. 9 the profiles for Fe, Cr, Ni, and Si in the UHP + Si alloy are plotted. The average concentrations at the boundary were 14.4 at% Cr, 13.1 at% Ni, and 3.2 at% Si. Fe segregation in the boundary region was observed by STEM, but due to difficulties in obtaining intergranular fracture, no corresponding AES data are available. These AES and STEM comparisons are summarized in fig. 5. Further details of the AES and STEM analyses will be provided in ref. [17].

In the present study, measurements by STEM have found 1.4 at% P at the boundary, which is significantly less than the 8.7 at% measured by AES. Calculations indicate that, for an assumed exponential P profile and a boundary value of 8.7 at% (the measured AES grain boundary concentration of P), the integrated concentration of P in the STEM measured profile should lie within the first two monolayers on both sides of the grain boundary. This is much smaller than estimates of the beam broadening, hence the entire P profile should be contained in the single grain boundary data point for STEM measurements and the P signal will be diluted by the probe size and beam broadening. Further details of the correlation of AES and STEM measurements of grain boundary segregation in the same alloy will be discussed in a forthcoming publication [17].

Nickel enrichment ratios and chromium depletion ratios for the alloys in the current study ranged from 1.4 to 1.75 and 0.7 to 0.85, respectively. Similar effects have been observed in type 304 stainless steel under light water reactor irradiation conditions. All neutron irradiations in the following discussion were conducted in-core at a temperature of 288°C with doses estimated for neutrons having energies greater than 1 MeV. Chung et al. [33], using AES for a commercial purity type 304 steel neutron irradiated to ~ 3 dpa, observed ratios of 1.3 for Ni and 0.75 to 0.87 for Cr. Analysis of a high purity alloy, irradiated under the same conditions, indicated slightly higher Ni enrichment (ratio = 1.5) and Cr depletion (ratio = 0.4 to 0.52). Measurements by Jacobs et al. [34,35] on two commercial purity heats of type 304 steel irradiated to 4–5 dpa showed Ni enrichment of ~ 1.75 times the bulk and Cr depletion
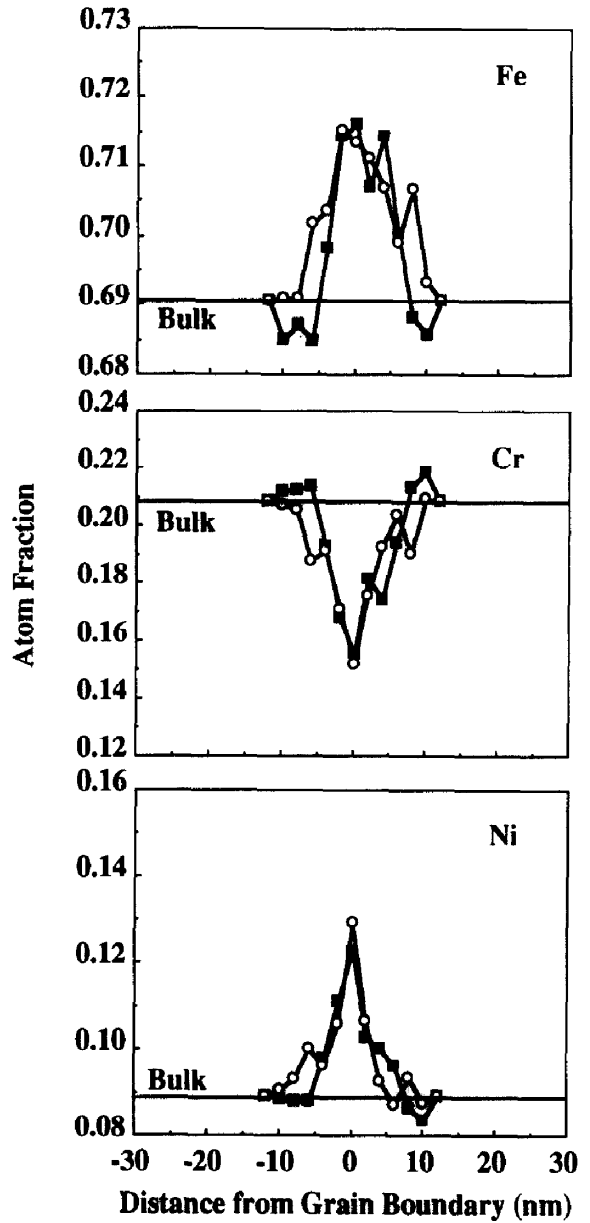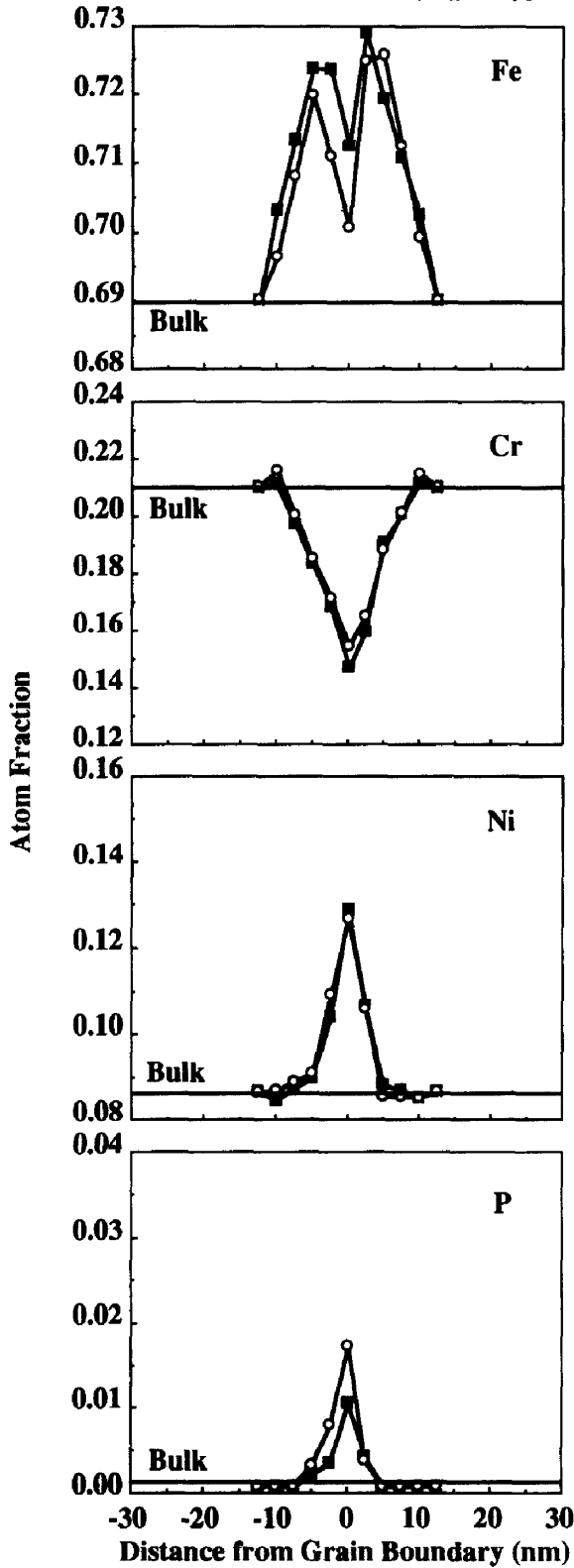

Fig. 6. STEM/EDS measured composition profiles across two grain boundaries in the UHP alloy irradiated with 3.4 MeV H$^+$ at 400°C to 1 dpa: (from the top down) Fe profile, Cr profile, Ni profile.

ary. The Cr and Ni redistribution, as observed in the UHP alloy, result in enrichment of Fe in the grain boundary region, however in the UHP + P and UHP + Si alloys, the Fe at the boundary is displaced by the presence of the impurity element.

Fig. 8. STEM/EDS measured composition profiles across two grain boundaries in the UHP + S alloy irradiated with 3.4 MeV H$^+$ at 400°C to 1 dpa: (from the top down) Fe profile, Cr profile, Ni profile.

Fig. 7. STEM/EDS measured composition profiles across two grain boundaries in the UHP + P alloy irradiated with 3.4 MeV H$^+$ at 400°C to 1 dpa: (from the top down) Fe profile, Cr profile, Ni profile, P profile.
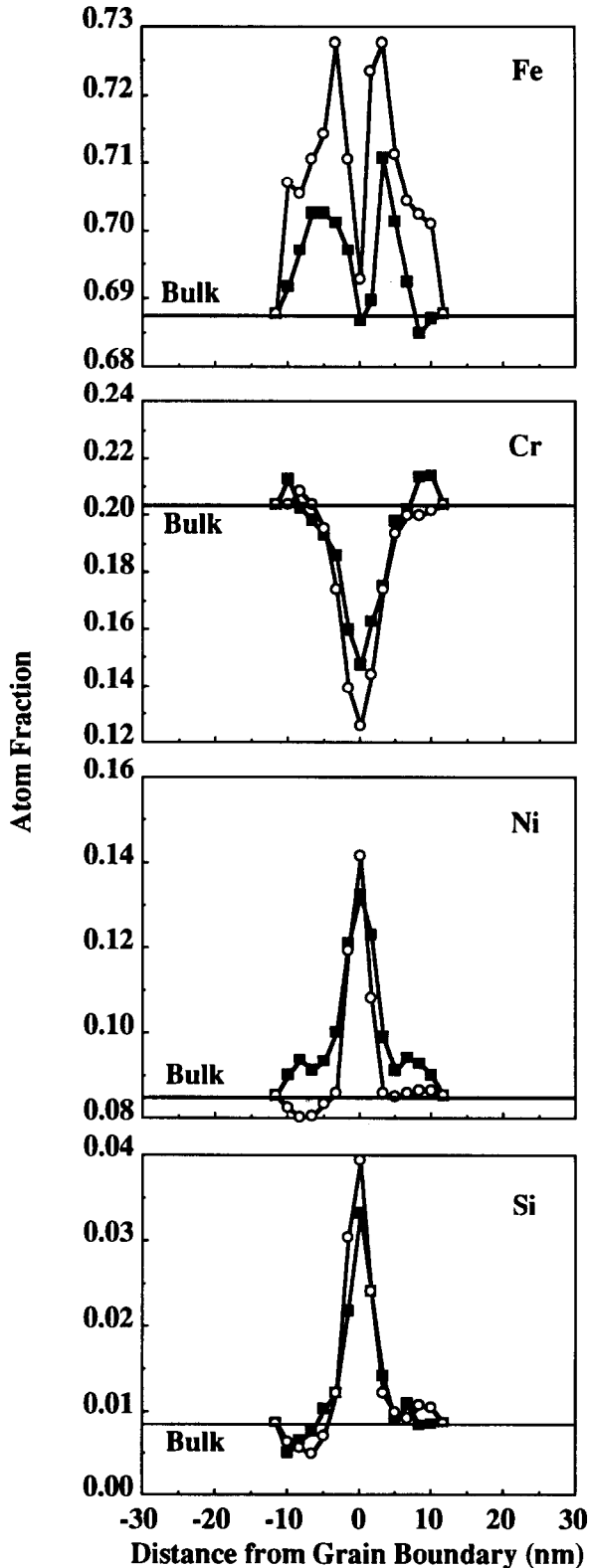
to between 0.75 and 0.85 times the bulk level. Analytical electron microscopy indicated that the Ni and Cr profile widths were on the order of 5 nm FWHM. Profile widths for the alloys in the present STEM study ranged from 3.5 to 6 nm FWHM. STEM/EDS examination of type 304 steel neutron irradiated to approximately 8 dpa by Asano et al. [36] showed Ni enrichment to 1.5 to 1.7 and Cr depletion to 0.85 times the bulk levels. Profile FWHM were approximately 5–10 nm.

Impurity segregation was also observed in the neutron irradiated stainless steels. Jacobs et al. [34,35] and Asano et al. [36] measured ~1 at% P at the grain boundary via STEM/EDS, as compared to measured values of 1.4 at% at the boundary of the UHP + P alloy in the present study. Chung et al. [33] observed strong segregation of both P and Si by AES in commercial purity type 304 steel. Si segregation to levels as high as 7 at% and 2–3 at% were observed by STEM/EDS at the grain boundary by Jacobs et al. [34,35] and Asano et al. [36] respectively. This is compared to 3.2 at% measured in the UHP + Si alloy in the present study. S segregation was observed using AES on several grain boundaries by Jacobs et al. [34,35] but not in other neutron-irradiation studies or in the UHP + S alloy in this work.

Comparison of the doped alloys to the UHP alloy indicated that the degree of major element redistribution is greater in the doped material. These observations are in conflict with the measurements by Chung et al. [33] which indicate stronger major element redistribution in a very high-purity alloy as compared to commercial purity material. Clearly the relationship between the major and minor element segregation behavior is not yet understood and further investigation is necessary.

4. Conclusions

Proton irradiation at 400°C to 1 dpa has been shown to produce microstructures and microchemistries similar to those produced in materials irradiated in-core. The network dislocation density increased by up to a factor of 15 (UHP + P) and loops

Fig. 9. STEM/EDS measured composition profiles across two grain boundaries in the UHP + Si alloy irradiated with 3.4 MeV H$^+$ at 400°C to 1 dpa: (from the top down) Fe profile, Cr profile, Ni profile, Si profile.

Atom Fraction

Distance from Grain Boundary (nm)

were present at $(5-9) \times 10^{21}$ m^{-3}, ranging in size from 14 nm (UHP + S) to 27 nm (UHP + P). The "black dot" loop density was $(6-9.5) \times 10^{21}$ m^{-3}. Radiation-induced depletion of chromium by 3.5–6 at%, and enrichment of nickel by 2.1–6.6 at%, was observed via both AES and STEM/EDS at the grain boundaries in all four alloys. Phosphorus enrichment at the grain boundaries was observed in the irradiated UHP + P to 8.7 at% by AES and 1.4 at% by STEM, and in the UHP + Si alloy silicon enrichment of 3.2 at% was observed at the boundaries. The degree of chromium and nickel segregation was greater in the doped alloys as compared to the UHP alloy, possibly indicating an interaction between the major and minor alloying elements. Thermal segregation of chromium and phosphorus to the grain boundaries and iron depletion at the boundaries were observed in the unirradiated UHP + P alloy.

Acknowledgements

References

[1] A.J. Jacobs and G.P. Wozadlo, Proc. Int. Conf. on Nuclear Power Plant Aging, Availability Factor and Reliability Analysis (ASM, Metals Park, OH, 1985) p. 173.

[2] H. Hanninen and I. Aho-Mantilla, Proc. 3rd Int. Conf. on Environmental Degradation of Materials in Nuclear

Power Systems – Water Reactors (The Minerals, Metals, and Materials Society, Warrendale, PA, 1988) p. 77.

[3] P.L. Andresen, F.P. Ford, S.M. Murphy, and J.M. Perks, Proc. 4th Int. Conf. on Environmental Degradation of Materials in Nuclear Power Systems – Water Reactors (National Association of Corrosion Engineers, Houston, 1990) p. 1.

[4] D.I.R. Norris, ed., Proc. Conf. on Radiation-Induced Sensitization of Stainless Steels (Central Electricity Generating Board, Berkeley, Gloucestershire, 1987).

[5] P.L. Andresen and F.P. Ford, Proc. Corrosion 89 (National Association of Corrosion Engineers, Cincinnati, OH, 1989) paper 497.

[6] D.I.R. Norris, C. Baker, and J.M. Titchmarsh, Proc. Conf. on Materials for Reactor Core Applications, vol. 1 (BNES, London, 1987) p. 277.

[7] G.R. Caskey, R.S. Ondrejcin, P. Aldred, R.B. Davis, and S.A. Wilson, Proc. Corrosion 90 (National Association of Corrosion Engineers, Cincinnati, OH, 1990) paper 504.

[8] A.J. Jacobs, G.P. Wozadlo, K. Nakata, T. Yoshida, and I. Masaoka, Proc. 3rd Int. Conf. on Environmental Degradation of Materials in Nuclear Power Systems – Water Reactors (The Minerals, Metals, and Materials Society, Warrendale, PA, 1988) p. 673.

[9] K. Fukuya, S. Nakahigishi, S. Ozake, M. Terasawa, and S. Shima, Proc. 3rd Int. Conf. on Environmental Degradation of Materials in Nuclear Power Systems – Water Reactors (The Minerals, Metals, and Materials Society, Warrendale, PA, 1988) p. 665.

[10] D.I.R. Norris, C. Baker, and J.M. Titchmarsh, Proc. Conf. on Radiation-Induced Sensitization of Stainless Steels (Central Electricity Generating Board, Berkeley, Gloucestershire, GL13 9PB, 1987) p. 86.

[11] P.L. Andresen and C.L. Briant, Proc. 3rd Int. Conf. on Environmental Degradation of Materials in Nuclear Power Systems – Water Reactors (The Minerals, Metals, and Materials Society, Warrendale, PA, 1988) p. 371.

[12] R.H. Jones, Proc. 2nd Int. Conf. on Environmental Degradation of Materials in Nuclear Power Systems – Water Reactors (American Nuclear Society, LaGrange Park, IL 1985) p. 173.

[13] D. Hull and D.J. Bacon, Introduction to Dislocations (Pergamon, Oxford, 1989) p. 22.

[14] J.F. Mansfield and D.C. Crawford, Proc. 12th Int. Conf. on Electron Microscopy, vol. 2: Analytical Sciences, eds. L.D. Peachy and D.B. Williams (1990) p. 504.

[15] P.J. Barton, B.L. Eyre and D.A. Stow, J. Nucl. Mater. 67 (1977) 181.

[16] M.H. Loretto and R.E. Smallman, Defect Analysis in Electron Microscopy (Chapman and Hall, London, 1976).

[17] R.D. Carter, D.L. Damcott, E.A. Kenik, J.R. Martin, G.S. Was and M. Atzmon, J. Nucl. Mater., submitted.

[18] C.L. Briant, Metall. Trans. 16A (1985) 2061.

[19] L.E. Davis, N.C. MacDonald, P.W. Palmberg, G.E. Riach and R.E. Weber, Handbook of Auger Electron Spectroscopy (Physical Electronics Division, Perkin-Elmer Corporation, Eden Prairie, MN, 1978).

[20] D.L. Damcott, J.M. Cookson, R.D. Carter, J.R. Martin, M. Atzmon and G.S. Was, Radiat. Eff. Def. Solids 118 (1991) 383.

[21] H. Fukushima, Y. Shimomura and H. Yoshida, J. Nucl. Mater. 141–143 (1986) 938.

[22] P.J. Maziasz and C.J. McHargue, Int. Mater. Rev. 32 (1987) 190.

[23] E.E. Bloom, W.R. Martin, J.O. Stiegler and J.R. Weir, J. Nucl. Mater. 22 (1967) 68.

[24] P.J. Maziasz, Effects of Helium Content on Microstructural Development in Type 316 Stainless Steel Under Neutron Irradiation, ORNL-6121 (1985).

[25] M.P. Tanaka, S. Hamada and P.J. Maziasz, Alloy Development for Irradiation Performance, Progress Report 23, DOE/ER-0045/16 (1985) p. 26.

[26] M.P. Tanaka, P.J. Maziasz, A. Hishinuma and S. Hamada, J. Nucl. Mater. 141–143 (1986) 943.

[27] M. Suzuki, S. Hamada and M.P. Tanaka, Fusion Reactor Materials, Progress Report 2, DOE/ER-0313/2 (1987) p. 213.

[28] C.L. Briant and H.J. Grabke, Mater. Sci. Forum 46 (1989) 253.

[29] C.L. Briant, Metall. Trans. 18A (1987) 691.

[30] M. Guttmann, P. Dumoulin, N. Tan-Tai and P. Fountaine, Corrosion 37 (1981) 416.

[31] G.S. Was and J.R. Martin, Metall. Trans. 16A (1985) 349.

[32] A.W. James and C.M. Shepherd, Mater. Sci. Technol. 5 (1989) 333.

[33] H.M. Chung, W.E. Ruther, J.E. Sanecki and T.F. Kassner, Proc. 5th Int. Conf. on Environmental Degradation of Materials in Nuclear Power Systems – Water Reactors (American Nuclear Society, LaGrange Park, IL, 1992) p. 795.

[34] A.J. Jacobs, G.E.C. Bell, C.M. Shepherd and G.P. Wozadlo, Proc, 5th Int. Conf. on Environmental Degradation of Materials in Nuclear Power Systems – Water Reactors (American Nuclear Society, LaGrange Park, IL 1992) p. 917.

[35] A.J. Jacobs, R.E. Clausing, L. Heatherly, and R.M. Kruger, Proc. 14th Int. Symp. on Effects of Radiation on Materials (American Society for Testing and Materials, Philadelphia, PA, 1989) p. 424.

[36] K. Asano, K. Nakata, K. Fukuya and M. Kodama, Proc. 5th Int. Conf. on Environmental Degradation of Materials in Nuclear Power Systems – Water Reactors (American Nuclear Society, LaGrange Park, IL, 1992) p. 838.